Formation of the Cassini Division -I. Shaping the rings by Mimas inward migration

Kévin Baillié, Benoît Noyelles, Valery Lainey, Sébastien Charnoz, G. Tobie

Monthly Notices
of the
ROYAL ASTRONOMICAL SOCIETY

MNRAS **486,** 2933–2946 (2019)
Advance Access publication 2019 February 25

doi:10.1093/mnras/stz548

Formation of the Cassini Division – I. Shaping the rings by Mimas inward migration

Kévin Baillié,[1]★ Benoît Noyelles,[2,3] Valéry Lainey,[1,4] Sébastien Charnoz[5] and Gabriel Tobie[6]

[1]*IMCCE, Observatoire de Paris, PSL Research University, CNRS, Sorbonne Universités, UPMC Univ Paris 06, Univ. Lille, 77 Av. Denfert-Rochereau, F-75014 Paris, France*
[2]*NAmur Institute for CompleX SYStems (NAXYS), University of Namur, Rempart de la Vierge 8, B-5000 Namur, Belgium*
[3]*Institut UTINAM, CNRS UMR 6213, Univ. Bourgogne Franche-Comté, OSU THETA, BP 1615, F-25010 Besançon Cedex, France*
[4]*Jet Propulsion Laboratory, California Institute of Technology, Pasadena, California, USA*
[5]*Institut de Physique du Globe, Sorbonne Paris Cité, Université Paris Diderot/CNRS, 1 rue Jussieu, F-75005 Paris, France*
[6]*Laboratoire de Planétologie et Géodynamique, Université de Nantes, CNRS, UMR-6112, Nantes, France*

Accepted 2019 February 16. Received 2019 February 14; in original form 2018 April 27

ABSTRACT

In 2017, the Cassini mission Grand Finale provided hints at the total mass of Saturn's ring system, constraining the age of the rings: they could actually be about 200 million years old or even younger. However, the present radial mass distribution across the rings is not well understood. The most prominent structure, visible from Earth, is the Cassini Division, a 4500 km-wide gap that separates the massive inner B ring and the outer A ring. Though early models of the formation of the Cassini Division suggested that the resonant interaction of ring particles with the external satellite Mimas (Lindblad resonance 2:1) could open a significant gap (slightly narrower than the observed Cassini Division) in 5 billion years, we investigate here an alternative scenario involving much shorter time-scales based on the new constraints on the age of the rings. In this article, we present a numerical model of satellite-ring interactions that can explain the formation of the Cassini Division by the orbital migration of Mimas and the different densities of the current A and B rings. Such a scenario implies that the Cassini Division could have opened in the last 4–11 million years and that it might disappear in the next 40 million years from now.

Key words: methods: numerical – planets and satellites: individual: Saturn – planets and satellites: individual: Cassini Division – planets and satellites: rings.

1 INTRODUCTION

The rings of Saturn present many variations of density, including interesting features like gaps and density waves. The most spectacular of these features is probably the Cassini Division that is a 4500 km-wide gap separating the A ring from the B ring. Theoretical studies suggest that these features are unstable over the age of the Solar system (Salmon et al. 2010). Moreover, some satellites of Saturn are known to have a dramatic impact on the architecture of the rings. In particular, the inner edge of the Cassini Division, i.e. the outer edge of the B ring, lies at the 2:1 mean-motion Inner Lindblad Resonance (ILR) with Mimas.

While the rings optical depth profile is well known, owing to the Cassini-UVIS stellar occultations in particular, the local surface mass density of material is only known in a few selected locations where density waves have been observed. The location and the azimuthal symmetry of an observed density wave relates to a given eccentric resonance with a satellite, allowing the density to be measured at the resonance location. These analyses lead to density values of about a few g cm^{-2} in the C ring (Baillié et al. 2011) and in the Cassini Division (Tiscareno et al. 2007; Colwell et al. 2009a; Baillié 2011), a few tens of g cm^{-2} in the A ring (Colwell et al. 2009b), up to a few hundreds of g cm^{-2} in the B ring despite its large opacity in some places that may prevent density wave observations (Hedman & Nicholson 2016).

Goldreich & Tremaine (1978) have proposed an explanation for the opening of the Cassini Division, by a static Mimas which would have been existing for the past 5 Gyr. The width of the Division would, in their process, be due to non-linear density waves in the rings, raised by

★ E-mail: kevin.baillie@obspm.fr

the resonance with Mimas. They suggested in particular that the size of the gap would be proportional to a quantity $t_R^{1/4}$, where t_R is the age of the rings. We know now, thanks to the Cassini Grand Finale, and in particular to measurements of the mass of the rings (Iess et al. 2017) and of the meteoritic bombardment, which should pollute the rings over the ages (Kempf et al. 2017), that the rings might be as young as 200 Myr old, instead of 5 Gyr. This prompts us to revisit the estimations of Goldreich & Tremaine (1978). Specifically, reestimating the age of the rings from 5 Gyr to 200 Myr induces a narrowing of the opened gap by a factor $(5\,\mathrm{Gyr}/200\,\mathrm{Myr})^{1/4} = 2.24$. While Goldreich & Tremaine (1978) could explain the formation of a gap as wide as the observed Cassini Division at the time (for which they estimated a width $\Delta r/r = 0.03$, i.e. ≈3525 km), this scenario applied to the new age of the rings would only explain a gap width of 1576 km. An additional widening of 3000 km still needs to be explained. In addition, numerical simulations from Schwarz (1981) showed that the Goldreich & Tremaine (1978) model could only open a gap smaller than 280 km, allowing to question the effectiveness of their model to open a 4500 km-wide gap as the Cassini Division.

We therefore propose an alternative scenario based on an orbital decay of Mimas. In a companion paper (Noyelles et al. 2019), hereafter named Paper II, we investigate two scenarios, which would explain a past inward migration of Mimas. The first scenario, named Scenario I, assumes that Mimas was initially trapped in a 2:1 mean-motion resonance with Tethys, which raised its eccentricity up to 0.2. Then the tidal heating resulting from this high eccentricity raised its temperature up to the melting point of water ice. At that point, the production of melt and subsequent formation of an internal ocean lead to a dramatic increase of its dissipation function k_2/Q. This resulted in an intense episode of dissipation in which Mimas migrated inward, before recrystallizing and resuming its outward motion that led to the currently observed inclination resonance with Tethys. Unfortunately, such a scenario would have melted the surface of Mimas, which is inconsistent with the observations of impact craters. Our second scenario, i.e. Scenario 2, is not based on a dissipation in Mimas, but in Enceladus, which is consistent with its geophysical activity. A dissipating Enceladus would have migrated inward, catching Mimas in a mean-motion resonance, the 3:2 and the 4:3 resonances being the most obvious candidates, and the two satellites would have both migrated inward. At the end of this process, the eccentricity of Enceladus would have been small enough to invert this motion, releasing Mimas and letting it be caught in the inclination resonance with Tethys. Unfortunately, this scenario requires the eccentricity of Enceladus to have reached 0.25, which would have destabilized the system of the mid-sized moons of Saturn. Based on those potential motions of Mimas, the associated 2:1 resonance will migrate inward as well, digging the Cassini Division. In this study, we simulate the linear response of the rings to this orbital motion with the 1D hydrocode HYDRORINGS (Charnoz, Salmon & Crida 2010; Charnoz et al. 2011). This code does not consider the non-linear emptying due to density waves, which would require a very fine grid, however we release the approximation of a constant density over time in the rings and the Cassini Division, by numerically integrating the viscous spreading of the rings material. Our simulations show that this may happen in a few million years only. However, the Cassini Division appears to be transient and will be refilled by viscous spreading in a few tens of million years, possibly slowed down by the ballistic transport of ring particles that may help maintain the outer edge of the Cassini Division while Mimas resumes an outward migration. Though Mimas' trajectory is extensively described in Paper II, we here detail the impact of Mimas' motion on the whole rings system.

In Section 2, we describe in detail our numerical hydrodynamical approach as well as our initial conditions. Section 3 studies the mechanisms at stake in the formation of the Cassini Division, while Section 4 investigates the future of the Division. Finally, Section 5 summarizes our conclusions and present perspectives for future work.

2 NUMERICAL MODELS

We study the impact upon the rings of the most prominent resonance associated with the satellite Mimas as it follows a synthetic orbital evolution: we investigate to which extent the orbital inward migration of the satellite can open a gap similar to the presently observed Cassini Division. We model the natural evolution of the rings using a viscous hydrodynamical code that accounts for the Lindblad resonance torques exerted by the satellites.

2.1 Rings evolution model

2.1.1 Rings evolution

In this study, we used the 'HYDRORINGS' code from Charnoz et al. (2010, 2011) that combines a one-dimension hydrodynamical code to model the rings surface mass density viscous evolution on one hand and a gravitational torque model that accounts for the moons-rings interaction on the other one. Though the approach is similar to the one detailed in Baillié & Charnoz (2014) and Baillié, Charnoz & Pantin (2015, 2016) for the viscous evolution of protoplanetary discs, there is no need of geometric, thermodynamic, and composition refinements in the case of Saturn's rings as the rings can be considered as a cold system of fixed composition to the present purpose. The HYDRORINGS code consists of a 1D finite elements code on a staggered mesh to compute the surface mass density of the rings that accounts for the gravitational back reaction of moons (gravitational torques are estimated from the formalism of Goldreich & Tremaine 1979, Lissauer & Cuzzi 1982, and Meyer-Vernet & Sicardy 1987). Though this code also includes an analytical orbital model to track the moons, we do not use such prescriptions on this work as we provide an external trajectory for Mimas: the time evolution of its semimajor axis is detailed in Section 2.3. The hydrodynamical part estimates the surface mass density on a grid of radii representing annuli and computes the mass fluxes at the edges

of each grid cell. In addition, though we do not allow material to flow inside the system, the rings can still yield material to the planet or beyond the Roche limit.

The hydrocode is a one-dimension finite elements code using a staggered grid with 100 km-wide bins that follows the evolution of the density based on the mass and angular momentum conservation (Pringle 1981) and accounting for the gravitational back reaction of moons:

$$\frac{\partial \Sigma(r,t)}{\partial t} = \frac{3}{r}\frac{\partial}{\partial r}\left(\sqrt{r}\frac{\partial}{\partial r}\left(\nu(r,t)\,\Sigma(r,t)\sqrt{r}\right) - \frac{1}{3\pi\sqrt{\mathcal{G}M_Y}}\sqrt{r}T(r,t)\right), \tag{1}$$

where r is the distance from Saturn, $\Sigma(r, t)$ is the surface mass density, $\nu(r, t)$ is the local viscosity, $\mathcal{G}$ is the gravitational constant, M_Y is Saturn's mass, and $T(r, t)$ is the sum, over all the considered satellites, of the local Lindblad-resonance torque densities.

Though the code is able to follow the creation of moonlets at the Roche limit, we do not use that refinement and only consider Mimas in this study: we focus in this paper on the Cassini Division and the surrounding denser rings. Canup & Esposito (1995) and Karjalainen (2007) estimated that accretion would not be efficient below 138 000 km which allows us to neglect that effect in our simulations.

2.1.2 *Rings viscosity*

The density evolution relies on a viscosity model that considers three different viscous sources as described in Salmon et al. (2010):

(i) a translational or 'local' viscosity, $\nu_{\rm trans}$ (Goldreich & Tremaine 1978), due to the random motion of particles,
(ii) a collisional or 'non-local' viscosity, $\nu_{\rm coll}$ (Araki & Tremaine 1986; Wisdom & Tremaine 1988).
(iii) a gravitational viscosity, $\nu_{\rm grav}$, due to the presence of self-gravity wakes (Salo 1992, 1995; Richardson 1994; Daisaka & Ida 1999; Ohtsuki & Emori 2000; Daisaka, Tanaka & Ida 2001).

We note $r_{\rm p}$, $m_{\rm p}$, and $\rho_{\rm p}$, the particle radius, mass, and density. $\tau = 3\Sigma/(4r_{\rm p}\rho_{\rm p})$ is the optical depth, Ω the orbital frequency, and $\sigma_{\rm r}$, the particle radial velocity dispersion (given by the particle's surface escape velocity $\sigma_{\rm r} = \sqrt{\mathcal{G}m_{\rm p}/r_{\rm p}}$ according to discussions in Salmon et al. 2010). $r_{\rm H} = r\left(\frac{2m_{\rm p}}{3M_Y}\right)^{1/3}$ is the particle's Hill radius, with r, the distance to the planet.

We can then define the Toomre parameter (Toomre 1964):

$$Q = \frac{\Omega\,\sigma_{\rm r}}{3.36\,\mathcal{G}\,\Sigma}. \tag{2}$$

This parameter reflects the gravitational stability of the disc (self-gravity wakes form for $Q < 2$).

Then the various viscosity contributions can be written as

$$\nu_{\rm trans} = \begin{cases} \frac{\sigma_{\rm r}^2}{2\Omega}\left(\frac{0.46\,\tau}{1+\tau^2}\right) & \text{if } Q > 2 \\ \frac{13}{32}\left(\frac{r_{\rm H}}{r_{\rm p}}\right)^5 \frac{\mathcal{G}^2\Sigma^2}{\Omega^3} & \text{if } Q < 2 \end{cases}, \tag{3}$$

$$\nu_{\rm coll} = r_{\rm p}^2\,\Omega\,\tau\,, \tag{4}$$

$$\nu_{\rm grav} = \begin{cases} 0 & \text{if } Q > 2 \\ \nu_{\rm trans} & \text{if } Q < 2 \end{cases}. \tag{5}$$

2.1.3 *Satellite resonances*

In our simulations, we considered only the 2:1 eccentric resonance with Mimas by applying the resonant torque to the bin corresponding to the resonance location. This approach is valid as the damping length of the resonance is narrower than the ring bin width. Among the distant interactions between external satellites and rings, lower order Lindblad resonances are those most likely to create ring structures affecting the radial distribution of material. In this section, we only consider resonances with the main external satellites: Janus, Mimas, Enceladus, Tethys, Dione, Rhea, Titan, Hyperion, Iapetus, and Phoebe. We use the Lindblad torque expressions derived by Goldreich & Tremaine (1979) and Lissauer & Cuzzi (1982) in the case of an l: $(m - 1)$ Lindblad resonance:

$$T^{\rm L}_{l,m} = -m\pi^2\left[\Sigma\left(\frac{r{\rm d}D_L}{{\rm d}r}\right)^{-1}\left(\frac{r d\phi^s_{l,m}}{dr} + \frac{2n(r)\phi^s_{l,m}}{n(r) - \Omega^{\rm P}_{l,m}}\right)^2\right]_{r_{\rm L}} \tag{6}$$

where n is the mean motion of the ring particles, κ is their epicyclic frequency, $\Omega^{\rm P}_{l,m}$ is their pattern speed, and

$$D_{\rm L}(r) = \kappa(r)^2 - m^2(n(r) - \Omega^{\rm P}_{l,m})^2. \tag{7}$$

The Fourier components $\phi^s_{l,m}$ are evaluated from Brouwer & Clemence (1961) (ch. 15, p. 490) and Murray & Dermott (1999) (equations 6.244–6.246) using the Keplerian approximation of $n \approx \kappa$:

$$\phi^{\rm s}_{1,1} = -\frac{GM_{\rm s}}{a_{\rm s}}[b^m_{1/2}(\beta) - \beta] \tag{8}$$

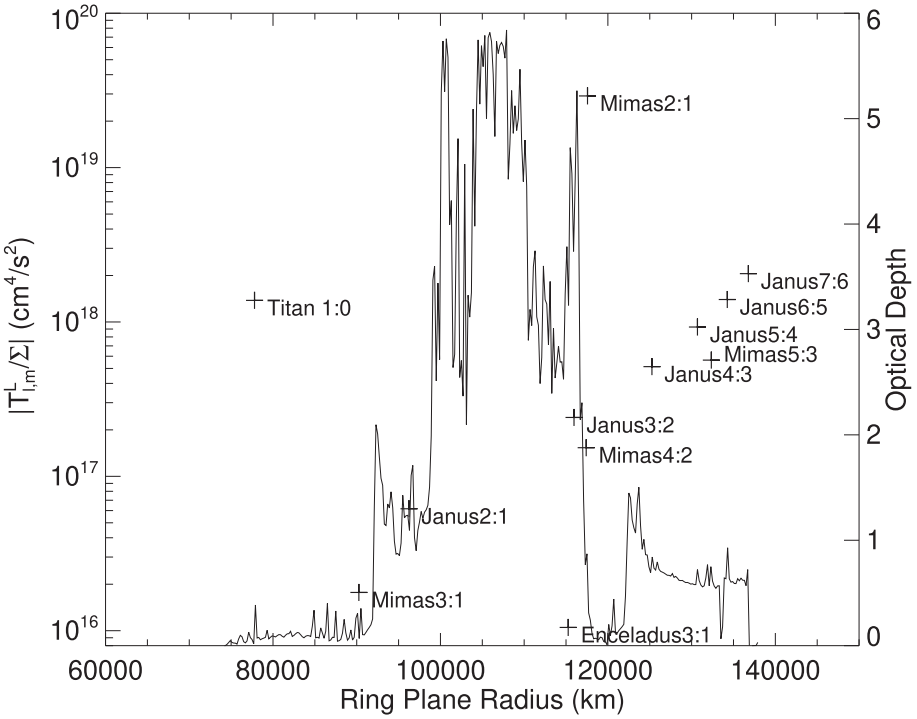

Figure 1. Location of the strongest resonances across the rings. We consider the main external satellites (Mimas and more massive). We present the ratio of the resonance torque intensity by the surface mass density together with the optical depth profile $\tau(r)$ of the rings for reference of the main ring structures (from Colwell et al. 2009b).

$$\phi^{\rm s}_{m,m} = -\frac{GM_{\rm s}}{a_{\rm s}} b^m_{1/2}(\beta),\ m > 1 \tag{9}$$

$$\phi^{\rm s}_{m+1,m} = -\frac{GM_{\rm s}e_{\rm s}}{a_{\rm s}} \left(\frac{1}{2} + m + \frac{\beta}{2}\frac{\rm d}{{\rm d}\beta}\right) b^m_{1/2}(\beta),\ m > 1 \tag{10}$$

$$\phi^{\rm s}_{m+2,m} = -\frac{GM_{\rm s}e^2_{\rm s}}{8a_{\rm s}} \left((4m^2 + m + 4) + (4m + 6)\beta\frac{\rm d}{{\rm d}\beta} + \beta^2\frac{{\rm d}^2}{{\rm d}\beta^2}\right) b^m_{1/2}(\beta),\ m > 1 \tag{11}$$

$$\phi^{\rm s}_{m+3,m} = -\frac{GM_{\rm s}e^3_{\rm s}}{48a_{\rm s}} \left((8m^3 + 42m^2 + 65m + 27) + (12m^2 + 51m + 51)\beta\frac{\rm d}{{\rm d}\beta} + (6m + 15)\beta^2\frac{{\rm d}^2}{{\rm d}\beta^2} + \beta^3\frac{{\rm d}^3}{{\rm d}\beta^3}\right) b^m_{1/2}(\beta),\ m > 1. \tag{12}$$

In these expressions, $a_{\rm s}$ and $e_{\rm s}$ are the semimajor axis and eccentricity of the perturbing satellite, $\beta = \frac{r}{a_{\rm s}}$ and $b^m_{1/2}(\beta)$ is the Laplace coefficient defined in equation (13), that is estimated numerically.

$$b^m_{1/2}(\beta) = \frac{2}{\pi}\int_0^\pi \frac{\cos(m\theta)\,{\rm d}\theta}{\left(1 - 2\beta\cos\theta + \beta^2\right)^{1/2}}\,. \tag{13}$$

We present the strongest resonances that are most likely to affect the present ring particles in Fig. 1.

We notice that the 2:1 resonance with Mimas clearly dominates by almost two orders of magnitude, followed by the first-order Lindblad resonances with Janus that are known to be associated with the density waves in the A (Baillié 2011) and B (Hedman & Nicholson 2016) rings, and by the Titan 1:0 apsidal resonance, whose impact on the rings is known to create the Titan ringlet (Porco et al. 1984). It appears that the only Lindblad resonances that may possibly compete with the Mimas first-order resonance are the first-order resonances associated with Janus in the outer A ring (which are suspected to be responsible for maintaining the outer edge of the A ring). However, the viscous

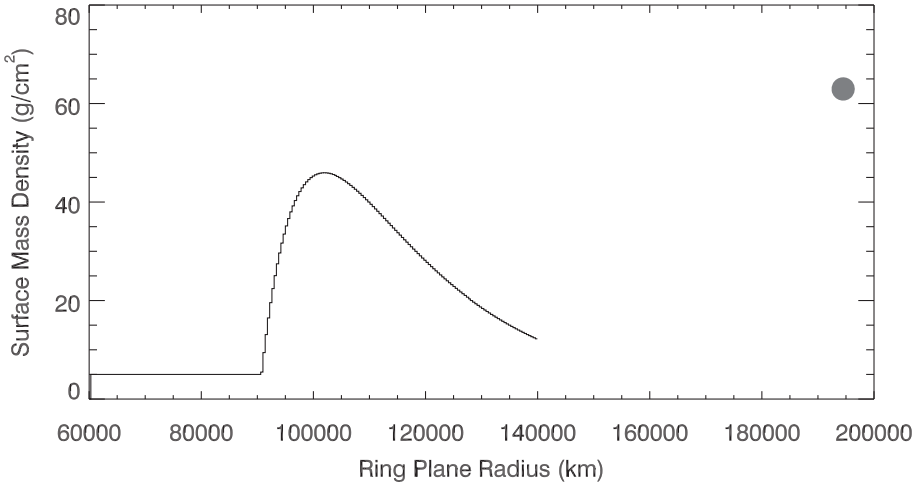

Figure 2. Initial ring density profile. The protoring between 92 000 and 140 000 km follows the profile described in equations (14)–(15).

spreading time-scales (Charnoz et al. 2009; Tajeddine et al. 2017) suggest that it is impossible for the material affected by the Janus first-order resonances beyond 135 000 km to interact with the material surrounding the Cassini Division over the age of the Solar system. Moreover, Charnoz et al. (2010) suggests that the most recent collision that formed Janus may be younger than 10 million years old, therefore restraining again the time of spreading of the material affected by the Janus resonances.

2.2 Rings initial conditions

2.2.1 Initial density

The initial ring density profile is presented in Fig. 2: we assume that the rings already formed and evolved for at least 10^8 yr following the 'standard' disc model described in Salmon et al. (2010), which is consistent with the new estimation of the age of Saturn's ring system. Our initial profile can be considered as the result of an evolved initial 3000 km-wide ring following a Gaussian density distribution centred at 110 000 km from the centre of the planet, with a ring mass about the mass of Mimas (see their paper for the initial ring mass discussion). Our initial density profile is given by

$$\Sigma(r) = \left(7.9\,10^{43}\,r^{-8.25}\,\ln\left(\tfrac{r}{90500\mathrm{km}}\right)\right)\ \mathrm{g\,cm^{-2}}\ \text{for}\ r > 90\,500\,\mathrm{km}, \tag{14}$$

$$\Sigma(r) = 5\,\mathrm{g\,cm^{-2}}\ \text{otherwise}, \tag{15}$$

with r in km.

The density values in the A and B rings are consistent with the present measurements of the surface mass density for the main rings: a few g cm^{-2} in the C ring (Baillié et al. 2011), a few tens of g cm^{-2} in the A ring (Colwell et al. 2009b), and up to a few hundreds of g cm^{-2} in the B ring (Hedman & Nicholson 2016). However, we added an initial C ring with a uniform density of 5 g cm^{-2}, consistent with the measured densities by Baillié et al. (2011). Therefore we assume that the C ring existed prior to the Cassini Division [consistently with the difference between the C ring particle size distribution (French & Nicholson 2000; Baillié et al. 2013) and the other rings] and investigate its survival through the Cassini Division opening process. It is worth noticing that we do not start with any formed gap across the rings.

2.2.2 Ring particles

We performed our tests with cm-sized particles. The size of the particles constituting the rings is expected to follow a power-law distribution, but the size of the particles does not affect the gravitational and translational viscosities, as long as the particles are significantly smaller than the gravitational-wake instability characteristic radial scale. We therefore chose an effective particle size of 1 cm.

Though the estimates of ring particle size distribution from Zebker, Marouf & Tyler (1985) and French & Nicholson (2000) tend to point towards the lower range of these values, Salmon et al. (2010) suggested to use metre-sized particles and Baillié et al. (2013) showed that metre-sized boulders are also common among the ring particles. However, as we model the rings as a hydrodynamical fluid rather than as individual particles, the size of these particles is considered as a viscosity parameter rather than as a dynamical scale. As shown in Salmon et al. (2010), a change in the particle radius affects the viscosity of the rings: the viscosity increases with particle radius in non-self-gravitating discs while the particle size will mostly affect the Toomre parameter in self-gravitating discs. Therefore, bigger particles would slow down the viscous spreading of self-gravitating discs and accelerate the evolution of non-self-gravitating rings.

2.3 Mimas' trajectory

In this paper, we study the impact of the 2:1 ILR with Mimas in the rings as the satellite migrates inward at first and outward after. Though the causes of these directions of migration are discussed in the companion paper (Paper II), we provide in the present section additional details regarding the consistency of these motions. We hypothesize that Mimas undergoes an orbital decay that lasts for a few million years. Then, in a second phase, Mimas resumes its outward migration, as presently observed. Therefore, we assume that the Cassini Division is not presently in its opening phase, but rather in a filling phase as its inner edge is currently likely moving outward.

2.3.1 Radial distance constraints

Based on the hypothesis that the 2:1 ILR with Mimas is actually at the origin of the Cassini Division, the resonance location must have at least migrated from the Cassini Division current outer edge (122 050 km) down to its current inner edge at 117 515 km (Colwell et al. 2009b). Assuming that the gap opening is only due to Mimas migration, this involves that Mimas also migrated inward, covering at least the interval from 192 699 to 185 539 km, namely over more than 7160 km.

In addition, Paper II shows that Mimas eccentricity cannot exceed 0.2 : such an eccentricity would result in a consequent internal heating so strong that it would not be compatible with the heavily cratered surface of Mimas (Plescia & Boyce 1982). This maximal eccentricity constrains the maximal extension of the satellite orbital decay by tidal migration to 9000 km, whatever the dissipation inside Mimas. Paper II also investigates the case of an inwardly migrating Enceladus in resonance with Mimas that pushes the latter inward. In such a case, the maximal eccentricity of Enceladus brings a similar constraint on the overall recession span of Mimas. Therefore, we can only test inward migration widths between 7160 and 9000 km that cover at least the range from 185 539 to 192 699 km.

However, when Mimas is inner to 192 699 km, the particles located at 122 050 km are no longer shepherded by the Mimas 2:1 ILR and they can spread into the Division owing to viscous spreading. This tends to slowly refill the Division and push its outer edge inward. Thus, it requires that the inward migration of Mimas began further than 192 699 km, so that the partial refilling of the Cassini Division by its outer edge does not bring it inner to its currently observed position. Initial tests showed that this requires to increase the inward migration phase by at least 800 km. Therefore, we investigate the two following scenarios: in the first one, we model the maximal migration of Mimas over 9000 km, while in the second one, Mimas migrates on a smaller range of 8000 km, though at a faster rate.

2.3.2 Phase 1: inward migration

The tidal evolution of the satellite semimajor axis a and eccentricity e is given by Kaula (1964), Yoder & Peale (1981), and Charnoz et al. (2011) who describe the competition between the tidal dissipation inside the planet at the forcing frequency of the satellite, noted $\left(\frac{k_2}{Q}\right)_{Y(\text{Mimas})}$, the tidal dissipation inside the satellite itself, noted $\left(\frac{k_2}{Q}\right)_{\text{Mimas}}$, and the disc torque on the satellite Γ_{disc}, where M_{M} is Mimas' mass, R_{M} is its radius, n is its mean motion, k_2 is Saturn's second-order Love number supposed constant, and Q is the dissipation factor, that varies with the forcing frequency (i.e. with the satellite mean motion mostly):

$$\frac{\mathrm{d}a}{\mathrm{d}t} = 3na\left(\frac{k_2}{Q}\right)_{Y(\text{Mimas})}\frac{M_{\text{M}}}{M_Y}\left(\frac{R_Y}{a}\right)^5\left(1+\frac{51}{4}e^2\right) - 21na\left(\frac{k_2}{Q}\right)_{\text{Mimas}}\frac{M_Y}{M_{\text{M}}}\left(\frac{R_{\text{M}}}{a}\right)^5 e^2 + \frac{2\Gamma_{\text{disc}}}{naM_{\text{M}}}, \tag{16}$$

$$\frac{\mathrm{d}e}{\mathrm{d}t} = \frac{57}{8}ne\left(\frac{k_2}{Q}\right)_{Y(\text{Mimas})}\frac{M_{\text{M}}}{M_Y}\left(\frac{R_Y}{a}\right)^5 - \frac{21}{2}ne\left(\frac{k_2}{Q}\right)_{\text{Mimas}}\frac{M_Y}{M_{\text{M}}}\left(\frac{R_{\text{M}}}{a}\right)^5. \tag{17}$$

Out of any resonance, Mimas' migration rate $\frac{\mathrm{d}a}{\mathrm{d}t}$ strongly depends on a competition between the dissipation inside the planet, assisted by the push of the rings, on one hand, and on the dissipation inside the satellite itself on the other hand. The second term can initially be neglected at low eccentricity (see equation 16). However, the total migration rate eventually becomes negative (synonymous of orbital decay) when either the $\left(\frac{k_2}{Q}\right)_{\text{Mimas}}$ inside Mimas or its eccentricity become large enough to compensate for the push of the rings and the $\left(\frac{k_2}{Q}\right)_{Y(\text{Mimas})}$ inside the planet. Though our code is able to take into account the disc torque on the rings, the counterpart of the rings on the satellite is not explicitly added as the satellite semimajor axis evolution is imposed by prescription. In fact, the adjustment of the tidal parameters that we perform implicitly compensates for this effect in order to provide the prescription for the satellite evolution.

Based on the synthetic evolutions of the orbit of Mimas presented in Paper II – fig. 1, we can estimate that $\frac{\Delta e}{e} \gg \frac{\Delta a}{a}$: therefore, we can consider that the eccentricity of the satellite evolves much faster than its semimajor axis. Thus, we may consider a constant semimajor axis $a = a_{\text{M}}$ and mean motion n in equation (17), for which the solution then reads

$$e(t) = e_0 \exp\left(-\frac{t}{\tau}\right), \tag{18}$$

with

$$\tau = \left[\sqrt{\mathcal{G}M_Y}\left(\frac{21}{2}\left(\frac{k_2}{Q}\right)_{\text{Mimas}}\frac{M_Y}{M_{\text{M}}}R_{\text{M}}^5 - \frac{57}{8}\left(\frac{k_2}{Q}\right)_{Y(\text{Mimas})}\frac{M_{\text{M}}}{M_Y}R_Y^5\right)\right]^{-1} a_{\text{M}}^{13/2}, \tag{19}$$

where e_0 is the initial eccentricity. When the satellite does not experience eccentricity forcing from the mutual perturbations, then e_0 is the maximal eccentricity, which is then damped by the tides. Injecting the solution (18) into the tidal equation for the semimajor axis evolution (16) finally gives

$$a(t) = \left(a_0^{13/2} + \frac{13}{2}\alpha t + \frac{13}{4}\tau e_0^2 \left(\frac{51}{4}\alpha - \beta \right) \left[1 - \exp\left(-\frac{2t}{\tau} \right) \right] \right)^{2/13}, \tag{20}$$

with

$$\alpha = 3\sqrt{\mathcal{G}M_Y} \left(\frac{k_2}{Q} \right)_{Y(\text{Mimas})} \frac{M_\text{M}}{M_Y} R_Y^5, \tag{21}$$

$$\beta = 21\sqrt{\mathcal{G}M_Y} \left(\frac{k_2}{Q} \right)_{\text{Mimas}} \frac{M_Y}{M_\text{M}} R_\text{M}^5. \tag{22}$$

We use this formula (20) to get synthetic trajectories of Mimas, by adjusting the initial eccentricity of Mimas e_0, and the two tidal coefficients $(k_2/Q)_{Y(\text{Mimas})}$ and $(k_2/Q)_{\text{Mimas}}$.

Another possibility is that Mimas could be in resonance with an outer satellite that would itself undergo such an inward tidal migration for similar reasons. Whether the inward migration of Mimas is due to an increase in its eccentricity, an increase in its dissipation, or a resonance with Enceladus for example is out of the scope of this paper and is presented in the companion paper. We call the inward migration 'Phase 1' and the following outward migration 'Phase 2'.

Considering an inward migration interval of $\Delta a = 9000$ km in 'Simulation 1', we set $\Delta t = 10$ million years since a longer migration time would result in a partial refilling of the Division from its outer edge. Our Simulation 1 then considers $e_0 = 0.25$, $(k_2/Q)_{Y(\text{Mimas})} = 1.96277 \times 10^{-4}$ and $(k_2/Q)_{\text{Mimas}} = 1.806 \times 10^{-4}$. These numbers result from fine-tuning of the tidal parameters. They are indeed very close to recent estimates from Lainey et al. (2017) for Saturn and from Paper II's appendix for Mimas.

Conversely, a faster migration of Mimas cannot push all the material of the proto-Cassini Division to empty it completely: some material remains in the gap. We refer to that phenomenon as 'particle leaking'. To limit the intensity of the leaking and allow the Division to form substantially, we also consider an orbital decay of 8000 km over 3 million years. This 'Simulation 2' takes $e_0 = 0.24$, $(k_2/Q)_{Y(\text{Mimas})} = 1.97302 \times 10^{-4}$ and $(k_2/Q)_{\text{Mimas}} = 4.853 \times 10^{-4}$. Our values for e_0 appear to exceed the maximal value of 0.2 for Mimas eccentricity (see Paper II), but if we considered the mutual perturbations, then the eccentricity of Mimas would be damped less efficiently because of the resonance, which is expected to raise the eccentricity. We therefore compensate by starting our simulations with a higher initial eccentricity. We can also notice that a faster decrease, such as the one in Simulation 2 compared to Simulation 1, requires a higher dissipation in Mimas.

2.3.3 Phase 2: outward migration

In the second phase, Mimas resumes its outward migration ($\frac{da}{dt} > 0$). This rate is supposed constant on average over that phase. Paper II discusses the possible causes of the inversion of the migration rate, investigating in particular the hypotheses of a drop of Mimas eccentricity, a change of state in its internal structure (and therefore a variation of its $\frac{k_2}{Q}$), an escape from a resonance with Enceladus, or even a resonance locking mode as suggested by Fuller, Luan & Quataert (2016). We assume that Mimas (and the Cassini Division) will reach their currently observed state during this Phase 2. This is reasonable since Mimas is obviously migrating outward presently.

In the case of a purely tidally driven outward migration of Mimas, we estimate $\frac{da}{dt} \sim 53$ km Myr^{-1}. However, Mimas is likely to get caught in resonance with Tethys as it is observed presently (Champenois & Vienne 1999a, b) during that phase 2. According to Paper II, this would slow down Mimas migration to $\frac{da}{dt} \sim 47$ km Myr^{-1}. We simulate this migration with the same tidal equation (20), in which e_0 is set to 0, $\left(\frac{k_2}{Q}\right)_{\text{Mimas}}$ disappears, and $\left(\frac{k_2}{Q}\right)_{Y(\text{Mimas})}$ is the same as in Phase 1.

2.4 Mimas' orbital evolution

The orbital evolution models of Mimas detailed in Section 2 are synthesized here: 'Simulation 1' involves an orbital inward migration of Mimas from 194 500 to 185 500 km in 10 million years (Fig. 3) while 'Simulation 2' brings Mimas from 193 500 to 185 500 km in 3 million years (Fig. 4). These trajectories allow to distinguish the two successive phases: an inward migration at first, followed by an outward migration. Though the phase transition is quite brutal in our analytical trajectories, this transition is certainly smoother in reality, therefore increasing slightly the elapsed time between the opening of the Division and the instant it reaches its current extension, with Mimas reaching its current observed semimajor axis at the same time.

Given the innermost location of Mimas in those trajectories and the average migration rate for Phase 2 (50 km Myr^{-1}), Mimas reaches its current location 730 000 yr after the end of the inward migration.

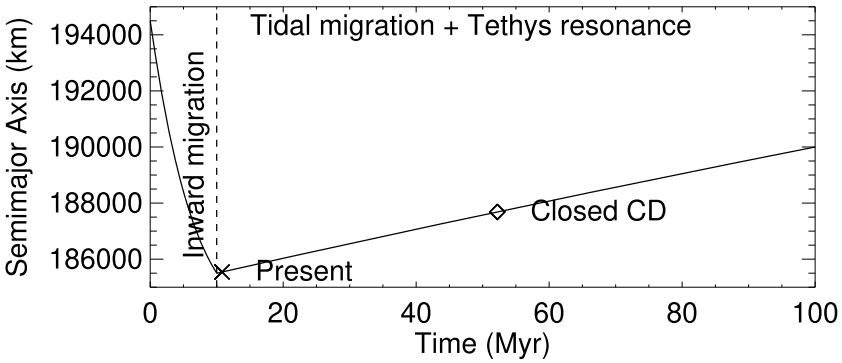

Figure 3. Evolution of Mimas' semimajor axis in 'Simulation 1', involving an inward regression of 9000 km over 10 million years. The vertical dashed line delimits the end of the inward migration phase. The '×' symbol shows the present configuration (matching the locations of Mimas and the Cassini Division), while the '◇' symbol stands for the moment when the Cassini Division will be refilled by the ring particles.

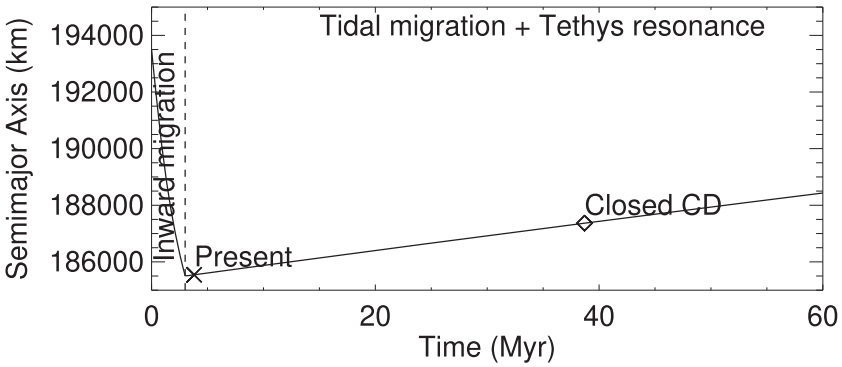

Figure 4. Evolution of Mimas' semimajor axis in 'Simulation 2", involving an inward regression of 8000 km over 3 million years. Legend is the same as Fig. 3.

3 RESULTS

3.1 Shaping the rings

The impact of Mimas' motion on the rings is presented in Figs 5 and 6: it shows the evolution of the rings surface mass density as Mimas moves according to the migration models detailed in Section 2. We notice that a gap appears early enough after the beginning of the simulation and that this gap reaches a width compatible with the observed Cassini Division in a few million years, around the end of Mimas' inward migration phase. In the meantime, the whole rings system is reshaped by the passing of Mimas' 2:1 resonance: though the density bump initially located around 100 000 km remains prominent throughout the simulation, additional features appear that remind us of the variety of ring structures observed presently.

Thus, Mimas' inward migration is sufficient alone to explain the formation of a gap located outer to its 2:1 resonance. However, explaining the present Cassini Division requires some adjustments regarding the duration of the two migration phases as well as the radial extension of the inward migration phase. At the inner edge of the proto-Division, the ring particles are pushed inward to accumulate and form an overdensity of material in the outer proto-B ring, which is now isolated from what will become the A ring. The outer edge of the gap remains localized at the position that the Mimas 2:1 resonance occupied when Mimas started its inward migration: the flux of the ring particles that spread across the outer edge into the Division does not compensate for the dilution of the mass density in the Division as the gap grows in width.

When Mimas resumes its outward migration, the gap gets slowly refilled. The inner edge moves outward following the resonance with Mimas, letting the ring particles of the outer proto-B ring flow into the space between the former and the newer resonance location. At the outer edge however, the proto-A ring particles flow freely into the Division: the ring material is no longer systematically brought to the inner edge by Mimas' inward migration. Thus, the Division fills in by both sides with the material accumulated on the neighbouring ring edges.

'Simulation 1' shows that Mimas reaches its current observed position after 10.73 million years. The corresponding ring density profile is presented in Fig. 7. Details of the formed Cassini Division (lower panel) exhibit a sharp inner edge at the 2:1 resonance with Mimas, a systematic emptying of the region between 117 500 km and 122 000 km that drops below 3 g cm^{-2}, and a smoother density transition at the outer edge, recalling the Cassini Division ramp observed in optical depth profiles (Colwell et al. 2009b).

Similarly, the current configuration of Mimas and the Cassini Division is reached in 3.73 million years in the case of 'Simulation 2' (Fig. 8). However, we notice that the density within the Cassini Division is slightly larger than for 'Simulation 1', around 5 g cm^{-2}. We

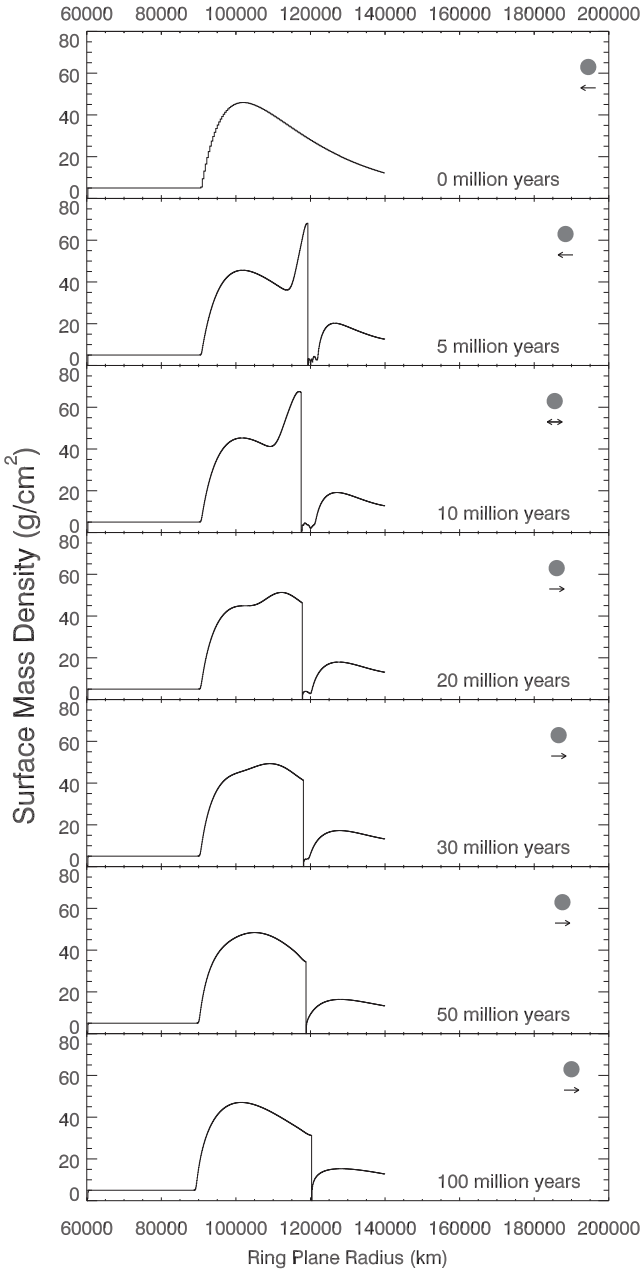

Figure 5. Evolution of the rings surface mass density for the trajectories of Mimas described in 'Simulation 1', with ring particles of 1 cm. At any time, Mimas' position is given by the grey dot and its direction of migration by the arrow below it.

interpret that as a more important 'leaking' phenomenon than in the previous case, likely owing to the larger inward migration velocity of Mimas and of its 2:1 resonance.

4 DISCUSSION

4.1 Density profile of the Cassini Division

Our simulations allowing to retrieve the right radial width and location of the Cassini Division, we now focus on the density distribution in and around the Division. Figs 7–8 show typical densities in the Cassini Division of a few g cm^{-2}, possibly forming substructures.

From the analysis of the Cassini data, Colwell et al. (2009a) and Baillié (2011) measured the following densities: from 0.98 to 1.31 g cm^{-2} (resp. 0.72 to 0.91) in the inner half of the Cassini Division, 5.76 g cm^{-2} (resp. 5.6) in the R10 ringlet defined in Colwell et al. (2009b), 3.51 g cm^{-2} in the Triple Band (resp. 2.9), and up to 15.4 g cm^{-2} (resp. 12.7) outer to the A ring ramp, where the optical depth is almost the one of the A ring, while Baillié (2011) additionally mentioned a density of 26.5 g cm^{-2} at 122 301 km in the A ring.

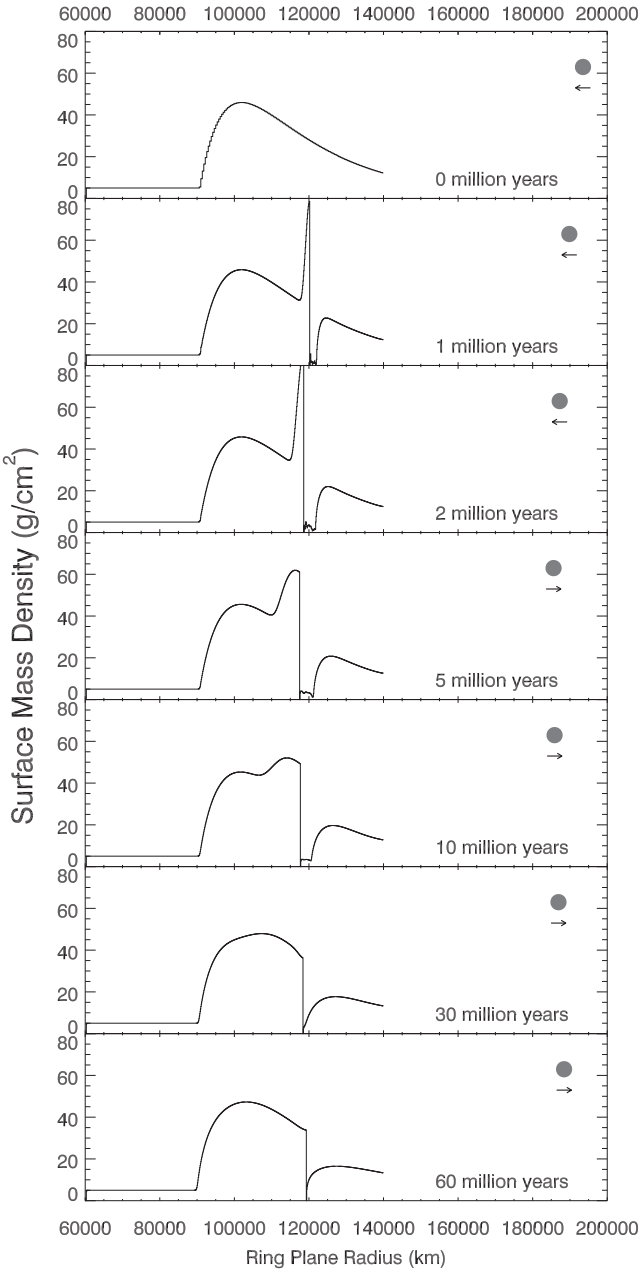

Figure 6. Same as Fig. 5 for 'Simulation 2'.

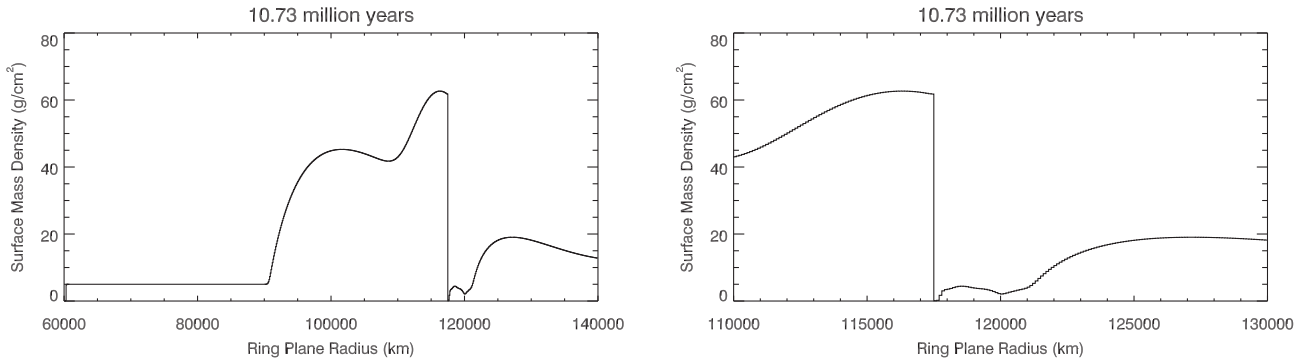

Figure 7. 'Simulation 1': Rings density profile after 10.73 million years of evolution, with ring particles of 1 cm. This date matches the present configuration of Mimas semimajor axis, the B ring outer edge, and the A ring inner edge.

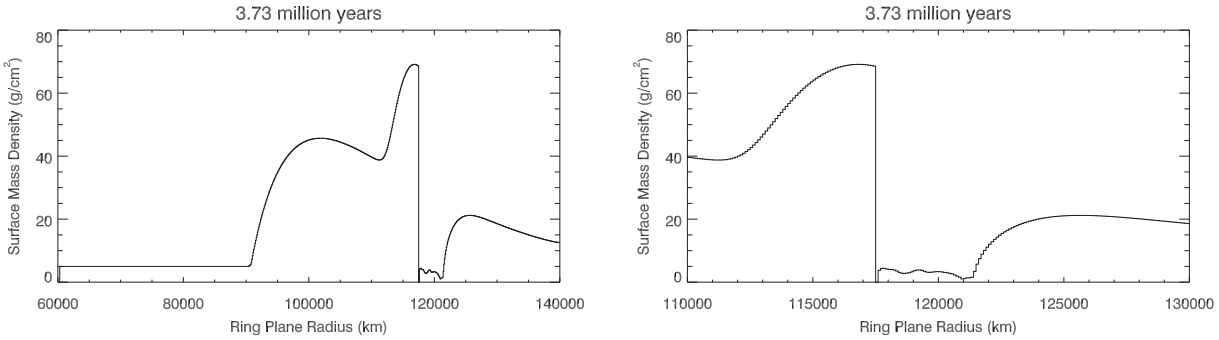

Figure 8. 'Simulation 2': Rings density profile after 3.73 million years of evolution, with ring particles of 1 cm, matching the current situation of the Cassini Division and Mimas.

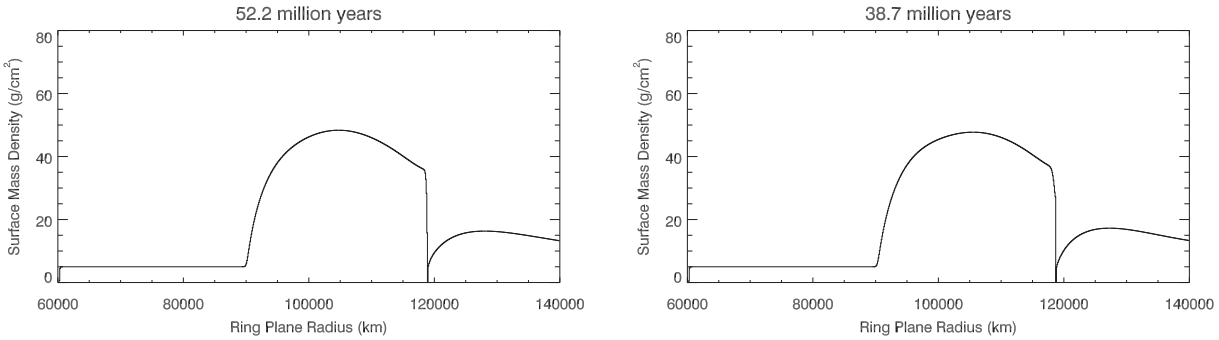

Figure 9. Ring density profile when the remnant gap (defined by a density lower than 5g cm^{-2}) becomes narrower than 100 km wide. This happens after 52.2 million years in 'Simulation 1' (upper panel) and after 38.7 million years in 'Simulation 2' (lower panel). At this date, the Cassini Division is now constrained to a remnant narrow gap located at the Mimas 2:1 ILR.

Assuming that the mass extinction coefficient is constant over the Cassini Division region, the density and optical depth profiles would be expected to be proportional, therefore allowing a direct comparison of the locations and heights of the bumps between these profiles.

We also observe substructures that might be due to the accumulation of material that leaked in the Cassini Division when the 2:1 resonance with Mimas pushed the rings material inward: this reminds us of the narrow ringlets observed in the current Cassini Division, such as the Huygens Ringlet located close to the inner edge of the Division.

4.2 Future evolution of the Cassini Division

Given that Mimas is now migrating outward, the inner edge of the Cassini Division is currently migrating outward towards its outer edge. That outer border is actually also moved inward, provided that the ballistic transport is not efficient enough, owing to the viscous spreading of the A ring particles that are not constrained inside the A ring by any resonance. Thus, the Cassini Division appears to be transient: though it reached its maximal width 730 000 yr ago (slightly wider than the current one), some material from the A ring is going to refill it by its outer edge over the next millions of years until it eventually reduces to a narrow gap located at the latest position of the Mimas 2:1 resonance.

Pursuing the numerical simulation beyond the current configuration of Mimas allows us to investigate the potential future configuration of the Cassini Division and the rings. We show in Fig. 9(a) that in 'Simulation 1', the Cassini Division gets refilled in less than 52.2 million years after its formation (i.e. less than 41.5 million years from now). At this stage the late Cassini Division will be located 118 950 km away from the centre of the planet. In 'Simulation 2', this happens just before 38.7 million years (i.e. 35 million years from now) and the late Cassini Division is located at 118 750 km (Fig. 9b).

4.3 Density structures across the rings

We notice that the location of an overdense region in the outer proto-B ring (around 115 000 km) coincides with the places where recent measurements have reported the largest densities across the rings (Hedman & Nicholson 2016). Though this density bump tends to smooth and disappear with time in our simulations, the average B ring density remains much larger than the average A ring density, in accordance with density measurements.

The C ring region does not appear to be affected substantially by Mimas' migration, which suggests that its existence and the fact that its density is much smaller than the other rings are older than the opening of the Cassini Division, which is consistent with the minimal age

of the C ring (> 15 million years) derived from the recent estimates of the silicates fraction measured from microwave observations (Zhang et al. 2017).

The junction between the Cassini Division and the A ring (characterized as a ramp in optical depth) was analysed from Cassini-VIMS observations (Nicholson et al. 2008) and Cassini-UVIS observations (Colwell et al. 2009a; Baillié 2011): opacity measures showed similar values in the Cassini Division ramp and in the A ring, consistently with models of ballistic transport (Durisen et al. 1989, 1992) suggesting that particles in the ramp may have drifted there from the A ring, as it happens in our simulations. This may then explain why the particle size distribution in the ramp is quite similar to the one in the A ring. Finally, we observe the accumulation of some ring material in the inner Cassini Division, a few hundred kilometres outer to the inner edge of the Division. Though we cannot pretend forming the Huygens Ringlet at this stage, the presence of material at the location where this ringlet is observed (around 117 850 km) is definitely a huge step in the understanding of the formation of the Cassini Division substructures.

4.4 Ring particles properties

The fact that the Cassini Division may have formed in a few million years can be consistent with a 'young rings' scenario without being necessarily opposed to a '4 billion-year old rings' scenario. This may explain why we still see structures in the Cassini Division, even though Esposito (1986) claimed that the viscous spreading of the A ring would prevent from sustaining the present structures over long time-scales. Indeed, we showed that Mimas' orbital motion actually reshapes the rings, no matter what structures were previously present.

In addition, radial variations of the colour ratio derived from Voyager colour images (Estrada & Cuzzi 1996; Estrada, Cuzzi & Showalter 2003) indicate that the Cassini Division is more contaminated by non-icy material than the A and B rings. Though our model is consistent with similar contaminations between the A and B rings as the ring particles spread from the A ring, across the Cassini Division, all the way to the outer B ring, it cannot explain alone the excess of pollution in the Cassini Division. None the less, particle size distributions derived from Voyager radio occultation (Zebker et al. 1985), ground-based observations of 28 Sgr-occultation (French & Nicholson 2000), and Cassini-UVIS stellar occultations (Baillié et al. 2013) present similar power-law index ($q \sim 2.75$) in the inner A ring, B ring, and Cassini Division, which is consistent with the fact that particles from the inner A ring migrated to the outer B ring.

4.5 Limitations on Mimas' evolution

Though 'Simulation 1' scenario allows to explain not only the formation of the Cassini Division, but also its actual width, it still requires to explain Mimas' trajectory to account for its current position and for the actual resonance with Tethys in which Mimas appears to be trapped presently. Paper II showed that such a trajectory may be obtained through different mechanisms, though with certain limitations.

One way to explain the orbital decay of Mimas would be to increase either its eccentricity, its internal tidal dissipation or both quantities. However, even though such a scenario explained most of the observational constraints (the resonance between Mimas and Tethys, Mimas' present eccentricity, and potentially the subsurface ocean of Mimas), the maximal eccentricity of Mimas before its inward migration should not exceed 0.2: a larger eccentricity would result in an internal heating so strong that Mimas would melt, therefore not allowing to explain the apparent heavily cratered surface of Mimas. In addition, this would affect the survival of Janus and Epimetheus that are located between Mimas and the rings, even though a late formation scenario of the coorbital satellites (Crida & El Moutamid 2016) could address this issue.

Paper II also describes another possible scenario for the orbital motion of Mimas: the satellite would be captured in a Lindblad resonance with Enceladus, which would be the one undergoing an inward orbital recession due to an increase in its eccentricity and/or tidal dissipation. Mimas would then be dragged inward by Enceladus' migration. As Enceladus is much larger than Mimas and obviously more active, the question of the internal heating is less problematic in that scenario: through its geysers, Enceladus is able to evacuate much more energy than Mimas, which would no longer need to melt entirely as in the previous scenario. At the very most, Mimas could receive the necessary energy to melt some subsurface layer of ice to form the ocean suggested by Tajeddine et al. (2014), without resurfacing the heavily cratered satellite. However, the strong eccentricity required to make the two satellites migrate inward over several thousands of kilometres makes it way more difficult for Mimas and Enceladus to remain trapped in resonance. In particular, after the resonance disruption, both satellites would need to get trapped in other resonances to match the present observations (Mimas with Tethys on one side and Enceladus with Dione on the other one).

Thus, even though the models that allow to explain Mimas' trajectories in our simulations are still showing some limitations, several mechanisms developed in Paper II suggest that Mimas must have migrated inward recently enough to open the Cassini Division.

5 CONCLUSIONS AND PERSPECTIVES

Based on the established presence of the 2:1 resonance with Mimas at the inner edge of the Cassini Division and on the current observational constraints, we have shown that an orbital inward migration of Mimas over a few thousand kilometres in a few million years can indeed create a gap whose size and position are similar to the ones of the current Cassini Division.

Although our hydrodynamic simulations of the rings are based on an ad hoc trajectory for Mimas that includes an orbital decay, serious leads have been developed to explain this trajectory for Mimas in the companion paper (Paper II). Based on the constraints imposed by the size and position of the Cassini Division, we estimate that this gap started forming between 3.73 and 10.73 million years ago, depending on the inward migration rate of Mimas. We also anticipate that the Division will get refilled in 35.0–41.5 million years from now.

The resonance with Mimas acts on the rings in the same way that a snow plow pushes the snow particles on a surface: it will push all the previous snow piles, leaving only the trace of the last passage of the snow plow. Similarly, current observations can only trace back the latest tack in Mimas' trajectory, without prejudice to the satellite's earlier history. In addition, depending on the inward migration rate of Mimas, more or less particles will pass over the shovel and settle on the road after the passage of the snow plow, i.e. more or less material of the rings will remain in the Cassini Division after the passing of Mimas' resonance. This 'leaking' phenomenon allows the formation of residual substructures in the gap dug by the resonance. It would be interesting to analyse more in depth this phenomenon, and to verify whether the Huygens ringlet, very close to the inner edge of the Cassini Division, could have formed this way.

Though the rings are covered by a continuum of resonances with the outer satellites, the 2:1 resonance with Mimas is clearly the strongest and the most able to create structures on the 1000-km scale. However, other higher order resonances with Mimas are able to shape other parts of the rings, and possibly even the outer edge of the massive rings (using low-order Janus resonances).

Finally, the problem of Mimas' trajectory connects with that of the internal structure of the satellites (Mimas or Enceladus depending on the scenario): the formation of subsurface oceans could be related to this inward migration phase at the origin of the Cassini Division. Paper II's discussions already provide us with many elements of response, although they do not yet allow us to construct a complete history of the satellites that would explain all the orbital, internal, and surface characteristics of the satellites; which will undoubtedly be the subject of a future paper.

ACKNOWLEDGEMENTS

KB acknowledges support of the Centre National des Études Spatiales (CNES). BN was supported by contract Prodex CR90253 from the Belgian Science Policy Office (BELSPO). VL's research was supported by an appointment to the NASA Postdoctoral Program at the NASA, Jet Propulsion Laboratory, California Institute of Technology, administered by Universities Space Research Association under contract with NASA. This collaboration, as part of the Encelade 2.0 working group, has been supported by the International Space Sciences Institute in Bern, Switzerland. We are indebted to J. Salmon for valuable suggestions and thorough reviews that improved the quality of the manuscript significantly.

REFERENCES

Araki S., Tremaine S., 1986, Icarus, 65, 83
Baillié K., 2011, PhD thesis, Univ. Central Florida
Baillié K., Charnoz S., 2014, ApJ, 786, 35
Baillié K., Colwell J. E., Lissauer J. J., Esposito L. W., Sremčević M., 2011, Icarus, 216, 292
Baillié K., Colwell J. E., Esposito L. W., Lewis M. C., 2013, AJ, 145, 171
Baillié K., Charnoz S., Pantin E., 2015, A&A, 577, A65
Baillié K., Charnoz S., Pantin E., 2016, A&A, 590, A60
Brouwer D., Clemence G. M., 1961, Methods of celestial mechanics. Academic Press, New York
Canup R. M., Esposito L. W., 1995, Icarus, 113, 331
Champenois S., Vienne A., 1999a, Celest. Mech. Dyna. Astron., 74, 111
Champenois S., Vienne A., 1999b, Icarus, 140, 106
Charnoz S., Dones L., Esposito L. W., Estrada P. R., Hedman M. M., 2009, in Dougherty M. K., Esposito L. W., Krimigis S. M., eds, Saturn from Cassini-Huygens, Springer Science, p. 537
Charnoz S., Salmon J., Crida A., 2010, Nature, 465, 752
Charnoz S. et al., 2011, Icarus, 216, 535
Colwell J. E., Cooney J. H., Esposito L. W., Sremčević M., 2009a, Icarus, 200, 574
Colwell J. E., Nicholson P. D., Tiscareno M. S., Murray C. D., French R. G., Marouf E. A., 2009b, in Dougherty M. K., Esposito L. W., Krimigis S. M., eds, Saturn from Cassini-Huygens, Springer Science, p. 375
Crida A., El Moutamid M., 2016, in AAS/Division for Planetary Sciences Meeting Abstracts. Vol. 48. p. 518.08
Daisaka H., Ida S., 1999, Earth Planets Space, 51, 1195
Daisaka H., Tanaka H., Ida S., 2001, Icarus, 154, 296
Durisen R. H., Cramer N. L., Murphy B. W., Cuzzi J. N., Mullikin T. L., Cederbloom S. E., 1989, Icarus, 80, 136
Durisen R. H., Bode P. W., Cuzzi J. N., Cederbloom S. E., Murphy B. W., 1992, Icarus, 100, 364
Esposito L. W., 1986, Icarus, 67, 345
Estrada P. R., Cuzzi J. N., 1996, Icarus, 122, 251
Estrada P. R., Cuzzi J. N., Showalter M. R., 2003, Icarus, 166, 212
French R. G., Nicholson P. D., 2000, Icarus, 145, 502
Fuller J., Luan J., Quataert E., 2016, MNRAS, 458, 3867
Goldreich P., Tremaine S. D., 1978, Icarus, 34, 240
Goldreich P., Tremaine S., 1979, ApJ, 233, 857
Hedman M. M., Nicholson P. D., 2016, Icarus, 279, 109
Iess L. et al., 2017, The dark side of Saturn's gravity. AGU Fall Meeting 2017 #U22A-03, New Orleans
Karjalainen R., 2007, Icarus, 189, 523
Kaula W. M., 1964, Rev. Geophys. Space Phys., 2, 661
Kempf S., Altobelli N., Srama R., Cuzzi J., Estrada P., 2017, The age of Saturn's rings constrained by the meteoroid flux into the system. AGU Fall Meeting 2017 #P34A-05, New Orleans
Lainey V. et al., 2017, Icarus, 281, 286

Lissauer J. J., Cuzzi J. N., 1982, AJ, 87, 1051
Meyer-Vernet N., Sicardy B., 1987, Icarus, 69, 157
Murray C. D., Dermott S. F., 1999, Solar System Dynamics. Springer, Berlin
Nicholson P. D. et al., 2008, Icarus, 193, 182
Noyelles B., Baillié K., Lainey V., Tobie G., Charnoz S., 2019, MNRAS, (companion Paper II)
Ohtsuki K., Emori H., 2000, AJ, 119, 403
Plescia J. B., Boyce J. M., 1982, Nature, 295, 285
Porco C., Nicholson P. D., Borderies N., Danielson G. E., Goldreich P., Holberg J. B., Lane A. L., 1984, Icarus, 60, 1
Pringle J. E., 1981, ARA&A, 19, 137
Richardson D. C., 1994, MNRAS, 269, 493
Salmon J., Charnoz S., Crida A., Brahic A., 2010, Icarus, 209, 771
Salo H., 1992, Nature, 359, 619
Salo H., 1995, Icarus, 117, 287
Schwarz M. P., 1981, Icarus, 48, 339
Tiscareno M. S., Burns J. A., Nicholson P. D., Hedman M. M., Porco C. C., 2007, Icarus, 189, 14
Tajeddine R., Rambaux N., Lainey V., Charnoz S., Richard A., Rivoldini A., Noyelles B., 2014, Science, 346, 322
Tajeddine R., Nicholson P. D., Longaretti P.-Y., El Moutamid M., Burns J. A., 2017, ApJS, 232, 28
Toomre A., 1964, ApJ, 139, 1217
Wisdom J., Tremaine S., 1988, AJ, 95, 925
Yoder C. F., Peale S. J., 1981, Icarus, 47, 1
Zebker H. A., Marouf E. A., Tyler G. L., 1985, Icarus, 64, 531
Zhang Z. et al., 2017, Icarus, 281, 297

This paper has been typeset from a TEX/LATEX file prepared by the author.